NON-UNIFORM ONSET OF NUCLEATE FLOW BOILING OF R-134A INSIDE A GLASS MINICHANNEL

Chiara Baldassari, Mauro Mameli, Marco Marengo[1]

Department of Engineering, University of Bergamo, Viale Marconi 5, Dalmine (BG), 24044 Italy, marco.marengo@unibg.it, Ph. +39 0352052002, Fax +39 0352052077

KEYWORDS

Flow boiling, onset nucleate boiling, flow pattern, HFC134a refrigerant

ABSTRACT

Even if far from being completely characterized, convective boiling inside mini- and micro-channels is likely to be one of the most relevant process for enhancing the cooling capability of modern heat transfer devices. Since, due to the process miniaturization, many novel devices are very small, fully developed flows are difficult to achieve, and therefore the knowledge of the onset nucleate boiling (ONB) position is even more critical for cooling design. However visualization of the ONB phenomena is not common in the literature, since usually the heaters are made in opaque metals and therefore they are not allowing a complete imagining. The present work consists in an experimental investigation of the incipient boiling of R134a inside a circular glass mini-channel mounted horizontally and equipped with a series of transparent Indium Tin Oxide (ITO) heaters. The effects of the heat flux input levels and the refrigerant mass fluxes on the ONB process and on the saturated boiling heat transfer rate are quantitatively explored. The flow pattern visualizations, carried on by means of a high-speed camera, show that the nucleation process is oddly non-uniform: the first vapor bubbles are always generated on the upper side of the tube and lead to a first wall temperature drop. A further increase in the heat flux values results in an increased wall superheat until bubbles nucleation originates also on the lower side of the tube causing a second wall temperature drop. Finally, at higher heat input levels, the boiling process becomes uniformly distributed on the inner tube surface. This phenomenon occurred also after a 180° rotation of the glass

[1] Corresponding author

tube and, after a critical analysis of the potential origins, it remains presently unexplained. An evaluation of the heat transfer coefficients for low vapor quality regimes is finally presented.

1. INTRODUCTION

Characterizing two-phase heat transfer phenomena inside mini and micro flow boiling systems is fundamental to understand how to increase the cooling capability of modern heat transfer devices. The need of an increased cooling capability is due to the smaller size of the components and the consequent higher specific heat generation. The complex nature of two-phase flows in mini and micro-channels needs still to be completely understood, as underlined by Thome [1,2], Celata [3], Harirchian and Garimella [4] and recently reviewed by Baldassari and Marengo [5]. After more than 30 years, flow patterns, void fraction measurement, heat transfer coefficient evaluation, onset of nucleate boiling are still open research topics for the flow boiling in mini and microchannels [5,6]. Focusing on the ONB, which marks the boundary between the single-phase and two-phase heat transfer region, Ghiaasiaan et al. [7] developed a semi-empirical method for the estimation of the incipient boiling heat flux. Bang et al. [8] performed a digital photographic study of subcooled flow boiling to observe near-wall structures, giving primary attention to bubble formation and bubble coalescence in the bubble layer. Callizo et al. [9] presented boiling curves for R-134a and a comparison between the experimental heat transfer coefficients and the predictions from classical correlations. Liu et al. [10] investigated experimentally ONB of water in a rectangular micro-channel developing an analytical model able to predict the heat flux and the bubble size at the onset of boiling. Recently, Hong et al. [11] found that the heat flux and wall superheat needed to initiate the nucleate boiling in narrow rectangular channel under static conditions, increased with the mass flux and the inlet subcooling.

The present paper focuses on the experimental analysis of the heterogeneous onset of nucleate flow boiling of R-134a in a mini-channel having 4 mm internal diameter, with a particular non symmetrical physical outcome, which is making the present research inspiring further investigations. In fact the use of a transparent glass tube with transparent heaters allows the visualization of the ONB and evidences a gradual activation of the nucleation sites, starting from the upper side of the heater to the lower side, for all the tested mass flux. The corresponding boiling curves evidence two different temperature drops, associated to the starting of the nucleation from the upper side and from the lower side of the heater, respectively. Two temperature drops have been also observed by Piasecka et al. [12] during

their boiling investigation. They found a two-stepped phase of the boiling phenomenon, similar to a second kind hysteresis, characteristic of nucleate pool boiling on developed micro-surfaces. They could not associate this kind of non-uniform condition to the flow pattern observation, since their experimental test-rig was not able to capture the bubble formation. In the present paper, ONB is visualized and recorded by means of a high-speed camera thanks to the ITO heaters, whose transparency allows a full characterization of the earliest stages of the bubbles formation. Several boiling curves are presented at different mass flux levels, G = 50, 80,100, 115 and 137 kg/m^{2}s together with the flow pattern visualization. Finally the heat transfer coefficient is calculated as a function of the heat flux and of the wall superheat for each mass flux.

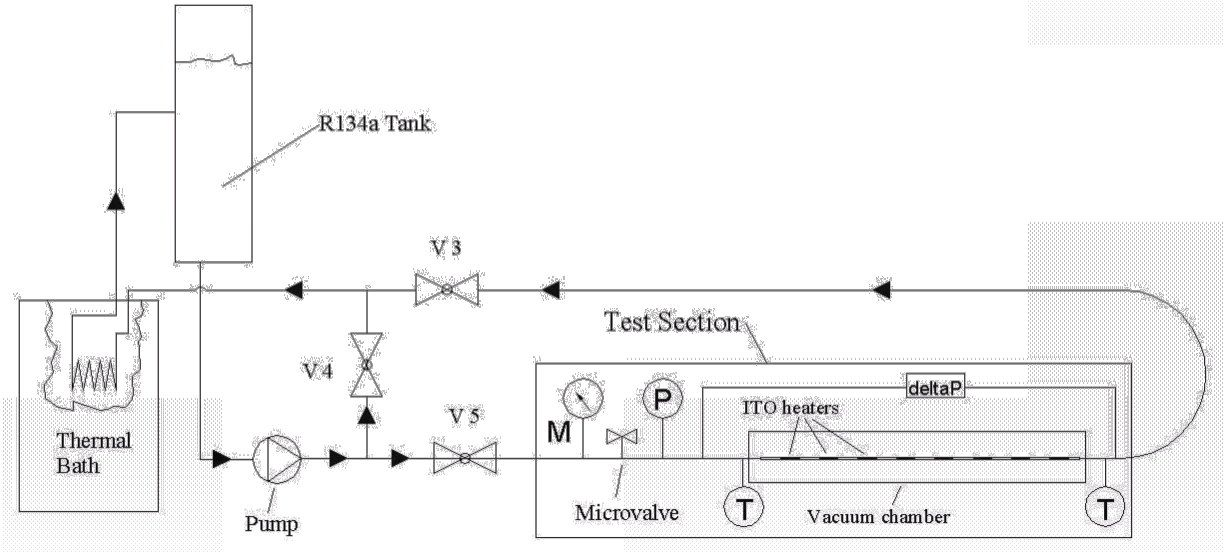

Figure 1 Experimental test rig scheme

2. EXPERIMENTAL SET-UP AND PROCEDURE

2.1 Experimental set-up

A schematic view of the experimental apparatus is given in Figure 1. The test section tube is made of high precision glass (DURAN) with an internal diameter of 4 mm. The Eotvos number $Eo = g(\rho_L - \rho_V)L^2/\sigma$ is hence set to 21.7, i.e. the flow boiling process is studied in the so-called macroscale region. The transparent ITO film covers eight portions of equal length (40 mm) and each independent portion is used to electrically heat the glass surface allowing to observe and record the boiling mechanisms taking place inside the tube with a high speed PCO® camera. The minichannel is enclosed in a co-axial glass tube with 60mm external diameter vacuumed in order to eliminate the convection heat losses and consider only

radiation losses. The temperature of the tube wall is monitored by means of eight K-type thermocouples (±0.2°C after calibration) placed externally on each heater at the upstream side and at the middle of the tube height, as represented in Figure 2.

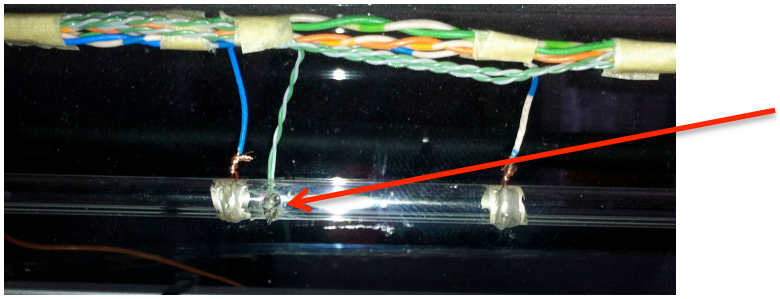

Figure 2 ITO heater and the position of the K-type thermocouple

During this experimental campaign one heater with a heat flux up to 30 kW/m^2 has been used. Refrigerant temperature is measured both at the test section inlet and outlet by two K-type thermocouples; the pressure is measured at the inlet by a PSE 510 pressure sensor.

The test rig consists of two main circuits: the test refrigerant loop and a secondary loop, where the fluid is thermally controlled. The loop is filled with R134a until the internal pressure reaches 6 bar, in order to bring the saturation temperature just below the ambient temperature. A helix type heat exchanger is cooled by means of a thermal bath HAAKE C50P®; this unit is necessary to define the operating experiment temperature and to condense the fluid coming from the test section in the form of wet vapor. The mass flow rate is measured by a Coriolis flow meter CORI-FLOW®. ITO coatings power is controlled by the PC through the NI (National Instruments) USB-6008® acquisition and control device and by the specifically designed electronic board, which is supplied with a 56V DC power supply. The electronic board applies the correct value of voltage to the heater in order to reach the desired electrical power and amplifies the coating voltage and current signals so that these can be acquired by the data acquisition module and transmitted to the PC. The radiation heat transfer between the ITO coating and the environment is numerically estimated and subtracted to the total power supplied to the ITO coatings in order to obtain the net thermal power supplied to the working fluid; this value is controlled with a standard PID (proportional-integral-derivative). Temperature and pressure signals are acquired using Agilent 34970A®. The system control, data acquisition software has been developed with Simulink® and dedicated MATLAB®

106 programs have been developed for the data post processing. Other details on the test rig are
107 given in [13].

108 **2.2 Experimental procedure**

109 Before running the experiments, the coaxial glass chamber is vacuumed, the mass flux is
110 adjusted to the desired value, the fluid inlet temperature is set in order to enter the test section
111 in sub-cooled condition of maximum 2K, and the system works as close as possible to the
112 saturated boiling conditions. The heater power supply is set to the desired value which is
113 maintained until a steady tube temperature is reached. Mass flux, temperature, pressure and
114 power input values are stored using the data acquisition system. In order to define the
115 characteristic boiling curves, the power supplied to the fluid is increased, starting from 0 W,
116 with increments of 0.5W in the regions near the onset of nucleate boiling, and of 1 W in the
117 other regions until the maximum power (Q_{max} = 11 W). Then the power level is decreased
118 from the maximum value to 0 W with step of 1 W. For each heat flux step, the corresponding
119 flow pattern is visualized and recorded using the high-speed camera. In order to provide the
120 necessary amount of light, a incandescent lamp is positioned in front of the camera. Because
121 the lamp temperature is very high, a glass covered with an infrared filtering film has been
122 located between the lamp and the test section, in order to minimize the radiated power.
123 The experimental procedure explained above is repeated two times for every mass flux value
124 examined, namely G = 50 kg/m^{2}s, G = 80 kg/m^{2}s, G = 100 kg/m^{2}s, G = 115 kg/m^{2}s and G =
125 137 kg/m^{2}s in order to check the repeatability. Finally the temperature difference, usually
126 called wall superheat, is calculated for each heat input level:

127 $$\Delta T_{sh} = T_{win} - T_{sat} \quad (1)$$

128 where $T_{w,in}$ is the internal temperature of the heated wall, and it is calculated starting from the
129 temperature of the external surface of the mini-channel measured by the single K-type
130 thermocouple in Figure 2, considering the heat conduction through the glass. T_{sat} is the fluid
131 inlet saturation temperature estimated with the help of the NIST REFPROP libraries [14],
132 knowing the fluid inlet pressure measured by the pressure sensor. Regarding the experimental
133 errors, the mass flow rate accuracy is ±1% while the pressure accuracy is ± 0.5% in the
134 pressure range of R-134a experiments (≈5.6 bar). The thermocouples have an accuracy of ±
135 0.2°C after calibration.

136 **3. EXPERIMENTAL RESULTS**

Thanks to the transparency of the ITO heaters, it is possible to visualize the earliest stages of the bubbles formation and the phase transition phenomena (Figure 3 and 4). The flow patterns visualization reveals that the first nucleation event always appears on the upper side of the heated tube for all the mass fluxes tested. Only after a further increase of the heat flux, the nucleation starts also on the lower side of the heated tube. When the nucleation appears, it is associated to a temperature drop. Hence the boiling curves presented in the next section evidence two temperature drops, that are respectively associated to the upper side and to the lower side onset of nucleate boiling.

The dimensionless numbers relative to the experimental conditions of Table 1 are given in Table 2.

Refrigerant	**Inlet pressure [MPa]**	**Tsat [°C]**	**G range [kg/m^{2}s]**	**q" [kW/m^2]**	**x [-]**
R-134a	0.537-0.590	18-21	50-137	0-22	max 0.093

Table 1 Summary of the experimental conditions

Specific mass flow rate	Liquid phase Capillary number	Liquid phase Reynolds number	Vapor phase Reynolds number	Boiling number	Confinement number
G	Ca(LO)	Re(LO)	Re(VO)	Bl	Cn
[kg/m^{2}s]	$Ca_{LO} = \frac{\mu_L G}{\rho_L \sigma}$	$\mathrm{Re}_{LO} = \frac{G d_h}{\mu_L}$	$\mathrm{Re}_{VO} = \frac{G d_h}{\mu_V}$	$Bl = \frac{q''}{G h_{fg}}$	$Cn = \left[\frac{1-x}{x}\right]^{0.9} \cdot \left[\frac{\rho_V}{\rho_L}\right]^{0.5}$
50	0.00097	975	17357	0.0024	1.161
80	0.00156	1560	27771	0.0015	1.479
100	0.00194	1949	34713	0.0012	1.803
115	0.00223	2242	39920	0.0011	2.155
137	0.00266	2671	47557	0.0009	3.023

Table 2 The dimensionless number values for the experimental conditions

3.1 Boiling curves and flow patterns

The heat flux versus ΔT_{sh} represents the boiling curve obtained during the experiments. In Figure 3 and 4 the boiling curves and the flow patterns corresponding to G = 115 kg/m^{2}s and G = 137 kg/m^{2}s are presented. The red line corresponds to the increasing in the heat flux, while the green line to the heat power decreasing. The boiling curves and the flow patterns corresponding to the other mass fluxes tested in this paper are presented in [15].

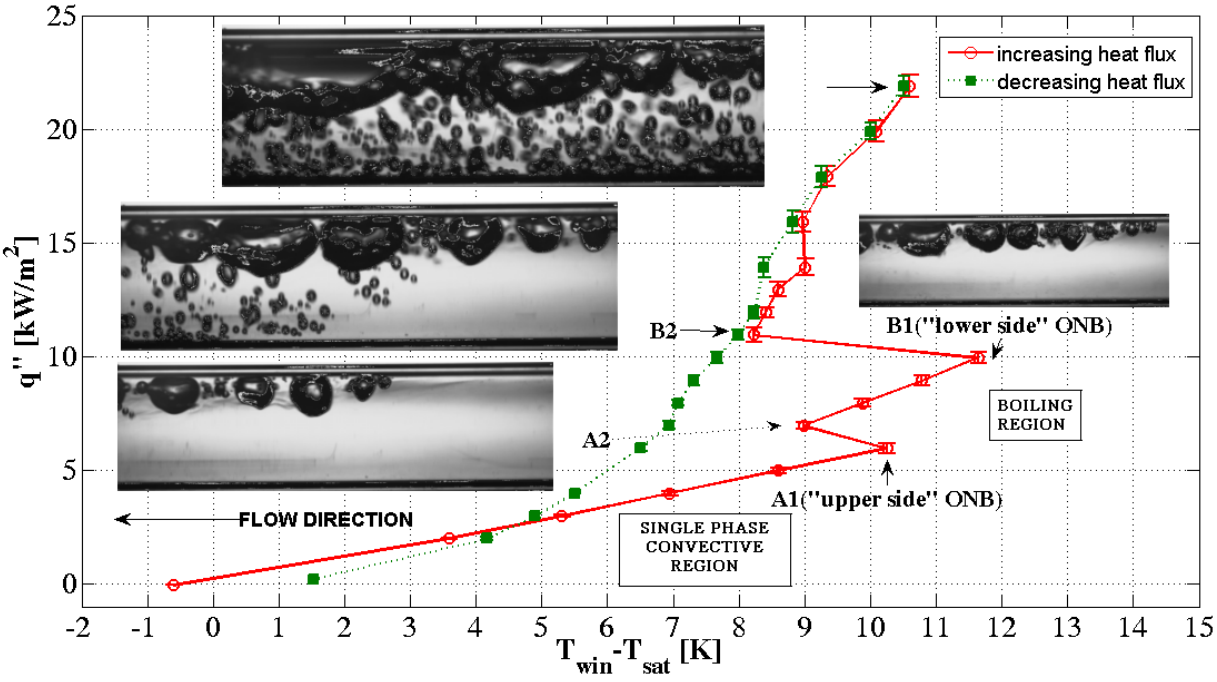

Figure 3 Boiling curve and flow patterns associated to points A2, B1, B2 and to q″=22 kW/m^2 for G=115 kg/m^{2}s and a maximum vapor quality of 0.04.

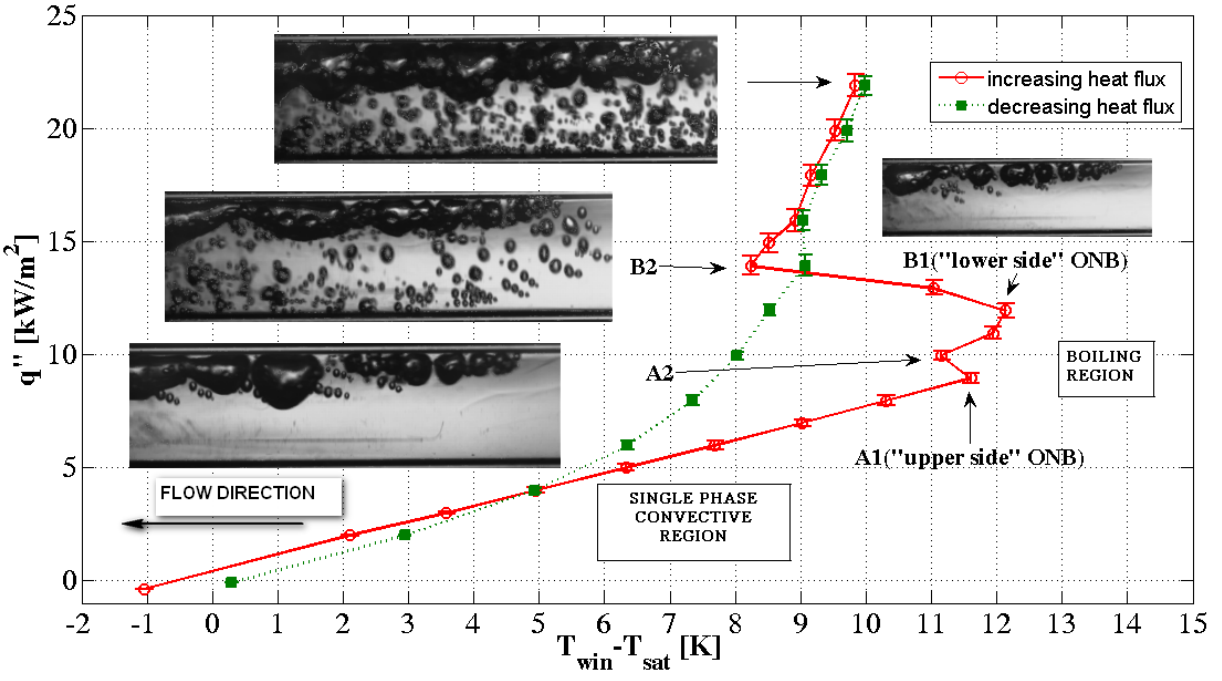

Figure 4 Boiling curve and flow patterns associated to points A2, B1, B2 and to q″=22 kW/m^2 for G=137 kg/m^{2}s and a maximum vapor quality of 0.035.

As usual, the values of wall superheat during the increasing of the heat flux are different from those obtained during the heat flux reduction ("boiling hysteresis"). Two main regions,

namely *single phase forced convective region* and *boiling flow region*, are clearly identified in the figures above. Regarding the red lines in Figure 3 and 4, the heat flux increases almost linearly with the increasing in the wall superheat in the single phase convective region. The liquid refrigerant in contact with the tube internal surface soon becomes superheated, whereas the fluid bulk may remain saturated or even slightly subcooled. Further increase in the heat flux results in an increased wall superheat; vapor nuclei are activated and the boiling process occurs in the upper side of the tube. The ONB heat transfer mechanism causes the heating surface temperature to drop, resulting in a reduction of the wall temperature (A2 in Figure 3 and 4). A further increase of the heat flux results in an increase of the number of bubble sites and the wall superheat is again slowly increasing.

In our experiment however a second temperature drop is clearly recognizable. From the visualizations it is possible to enlighten that this second temperature drop occurs when the nucleation starts also in the lower side of the heater. Hence such temperature drop (B2 in Figure 3 and 4) is due to a heterogeneous but non-uniform flow boiling process.

In order to further clarify the nomenclature A1, A2, B1, B2 used in the figures above, it is important to define:

- A1 as the "upper side" ONB point; it corresponds to the maximum heat flux value at which only liquid phase exists;
- A2 corresponds to the maximum temperature drop occurring after A1. Then a further increase of the heat input level results in an increase of wall superheat;
- B1 is the "lower side" ONB, defined as the maximum wall superheat below which boiling is still only activated in the upper side of the heater.
- B2 corresponds to the maximum temperature drop occurring after B1.

In B2 the nucleation starts also in the lower part of the heater. Afterwards boiling occurs more uniformly on both the upper and lower tube surfaces, and the red curve is showing a more regular trend, since the wall superheat increases almost linearly with the heat flux.

3.3 Hypothesis on the origins of non-uniform onset nucleate boiling

Four hypotheses were made by the authors to explain why in our experiment the nucleation always starts in the upper side of the heater:

- the hydrostatic difference of pressure between the upper side and the lower side of the heater could cause a difference in saturation temperature, which could be responsible for the non-uniform boiling;
- a different surface roughness of the glass tube could influence the nucleation process;

- the ITO coating could have been spattered with a non homogeneous thickness.

We have then achieved the following answers:

- the hydrostatic difference of pressure in a channel having 4 mm internal diameter at 20°C is forty times lower than the pressure needed to increase the saturation temperature of 1°C;
- the surface roughness of the glass is in the order of the nanometers and no scratch or defect is optically noticeable on the surface at least at the microscale;
- the "upper side" and the "lower side" ONB were observed repeating the experiment using all eight different ITO heaters in different positions along the tube;
- since the plasma coating procedure can originate the same non-uniformity for all the 8 heaters, the experiment was then repeated after rotating the tube of 180°. It was confirmed that the boiling always starts in the upper side of the heater.

Additionally the low thermal diffusivity of the glass, used for the tubes, is of course amplifying the effects of the non-uniform distribution of nucleation sites, since the internal wall conduction is not able to reduce thermal gradients.

A possible temperature gradient inside the refrigerant flow could be a reason for such phenomenon, even if the inlet of the minichannel is at least 600mm (150 D_i) far from the last geometrical change of the tube, which occurs just after the Coriolis flow meter, named M in Figure 1.

A further possibility to explore is that, because of the presence of gas inside the refrigerant, a number of gas molecules will accumulate in form of nanobubbles on the inner tube surface [16,17,18]. The presence of gas inside the refrigerant, according to the standard Ahri 700-2011, can be estimated as 1,5% vol at 298 K. Due to buoyancy forces the number of the nanobubbles will be higher on the top side with respect to the bottom side. These pre-existing air embryos entrapped in the flow and concentrated in the upper side of the mini-channel could be the responsible for the starting of the nucleation on the upper side.

3.4 Heat transfer coefficients

From each boiling curve obtained decreasing the heat flux, it was possible to calculate the heat transfer coefficient according to the equation:

$$q'' = h\,(T_{win} - T_{sat}) \qquad (2)$$

In Figures 5-7 the heat transfer coefficients are presented with the error bars; the uncertainties are calculated according to the theory of error propagation, starting from the errors on the heat

flux and on the wall superheat. In Table 3 the sensor accuracy and the estimated uncertainties of the derived quantities are summarized.

Sensors accuracy	Mass flow rate	Pressure (at ≈5.6 bar)	K-type thermocouples (after calibration)
	±1%	± 0.5%	± 0.2°C
Maximum estimated uncertainty	Heat flux	Wall superheat	Heat transfer coefficient
	±4%	±7%	±8%

Table 3 Summary of the sensor accuracy and the estimated uncertainties of the derived quantities

Boiling curves and the associated flow patterns for G = 50, 80 and 100 kg/m^{2}s are presented in [15]. It is important to point out that the data obtained for G= 50 kg/m^{2}s have the peculiarity that phase A1 may not correspond only to a single liquid phase, since first nucleation events may occurs even before, without a measurable variation of the wall superheat. This effect is due to the fact that a single thermocouple for each heater is not able to capture the local temperature variation around the bubble nucleation site. Such measurement weakness may produce larger experimental inaccuracies, even with the current high precision, especially for low wall superheat temperatures.

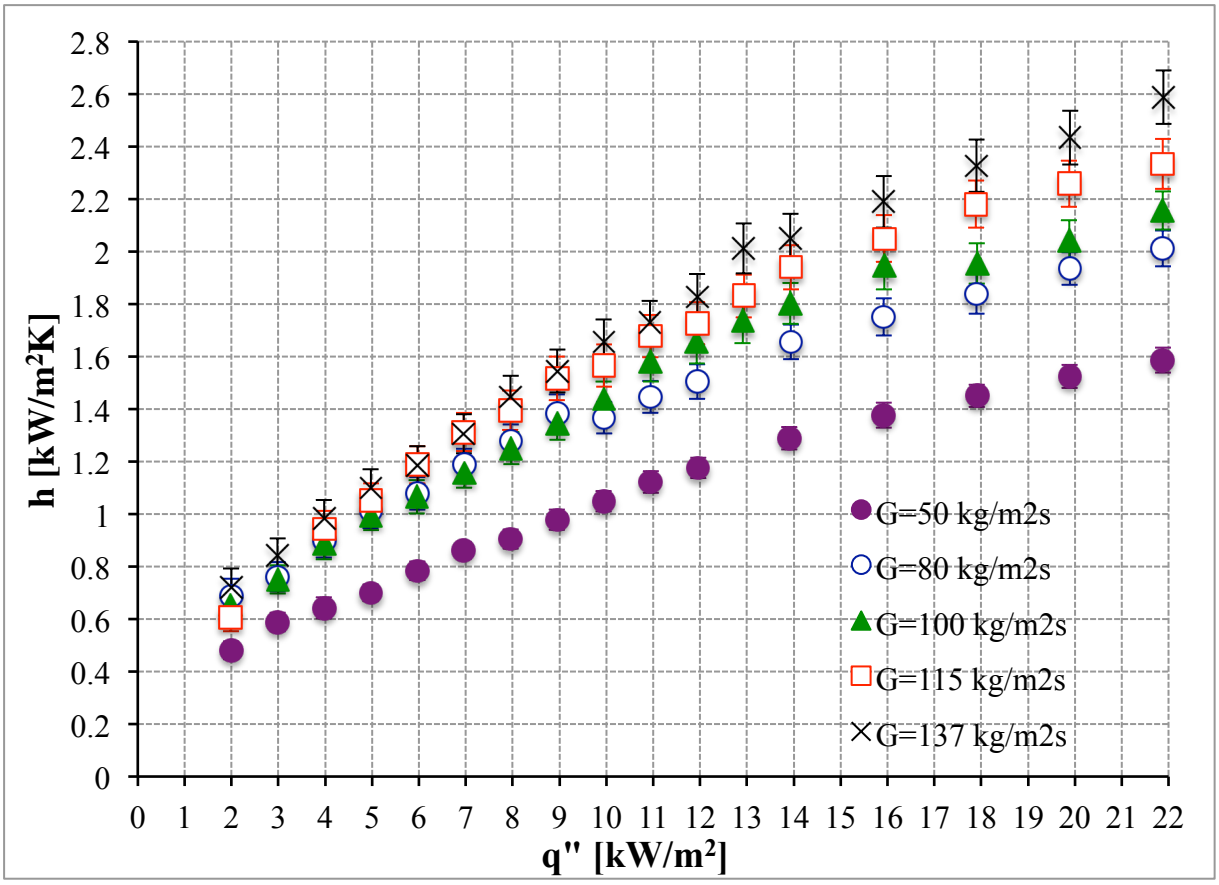

Figure 5 The heat transfer coefficient h, evaluated from each boiling curve - obtained decreasing the heat flux - as function of the heat flux.

In Figure 5 for a heat flux about 9 kW/m^2 the data obtained with G=100 kg/m^{2}s apparently decrease more than the data with G=80 kg/m^{2}s, keeping lower values until the minimum heat flux of 2 kW/m^2 is reached. Such a trend inversion is explained considering only the experimental accuracy, since there is no relevant change in the flow patterns.

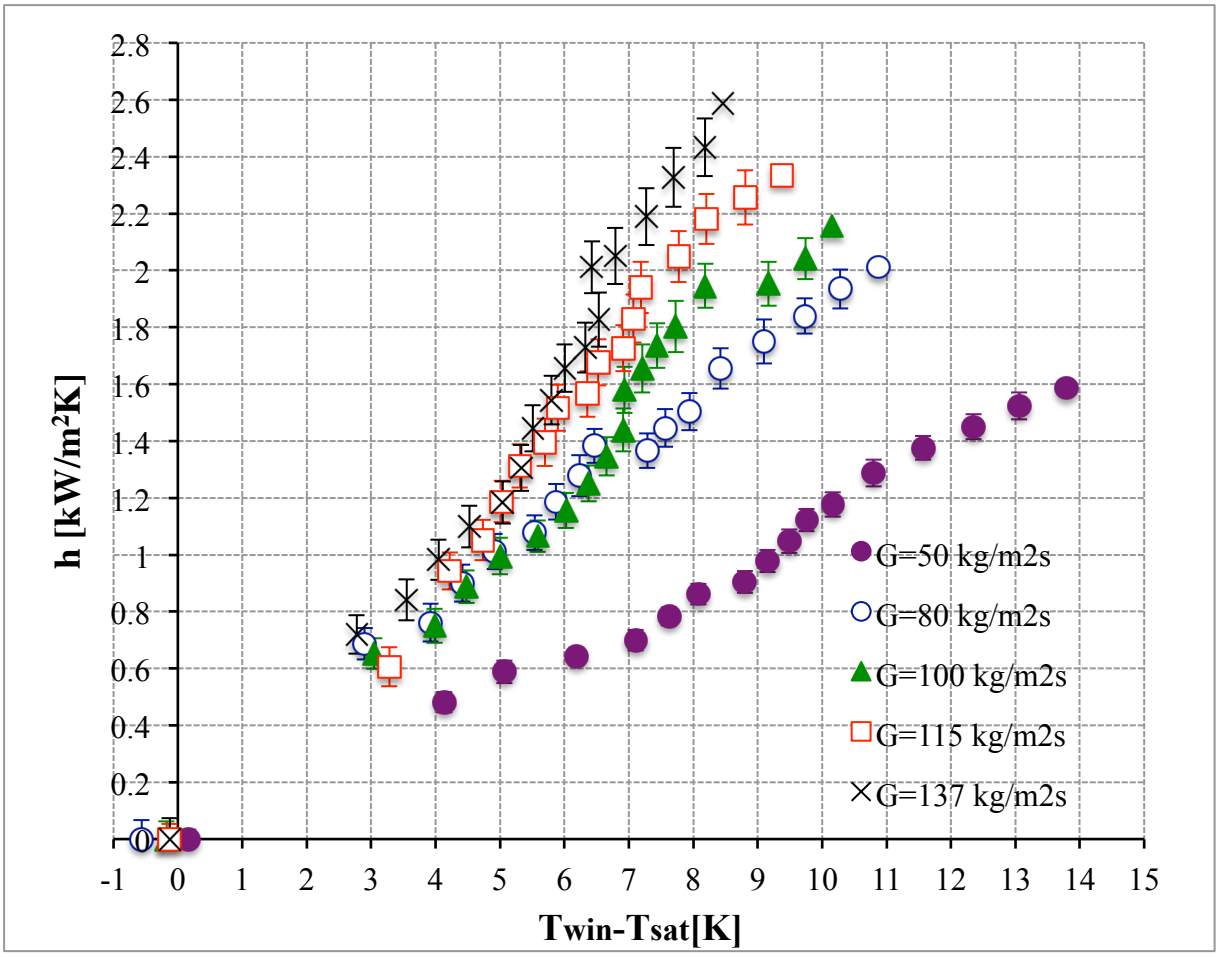

Figure 6 The heat transfer coefficient h, calculated from each boiling curve - obtained decreasing the heat flux - as function of the wall superheat.

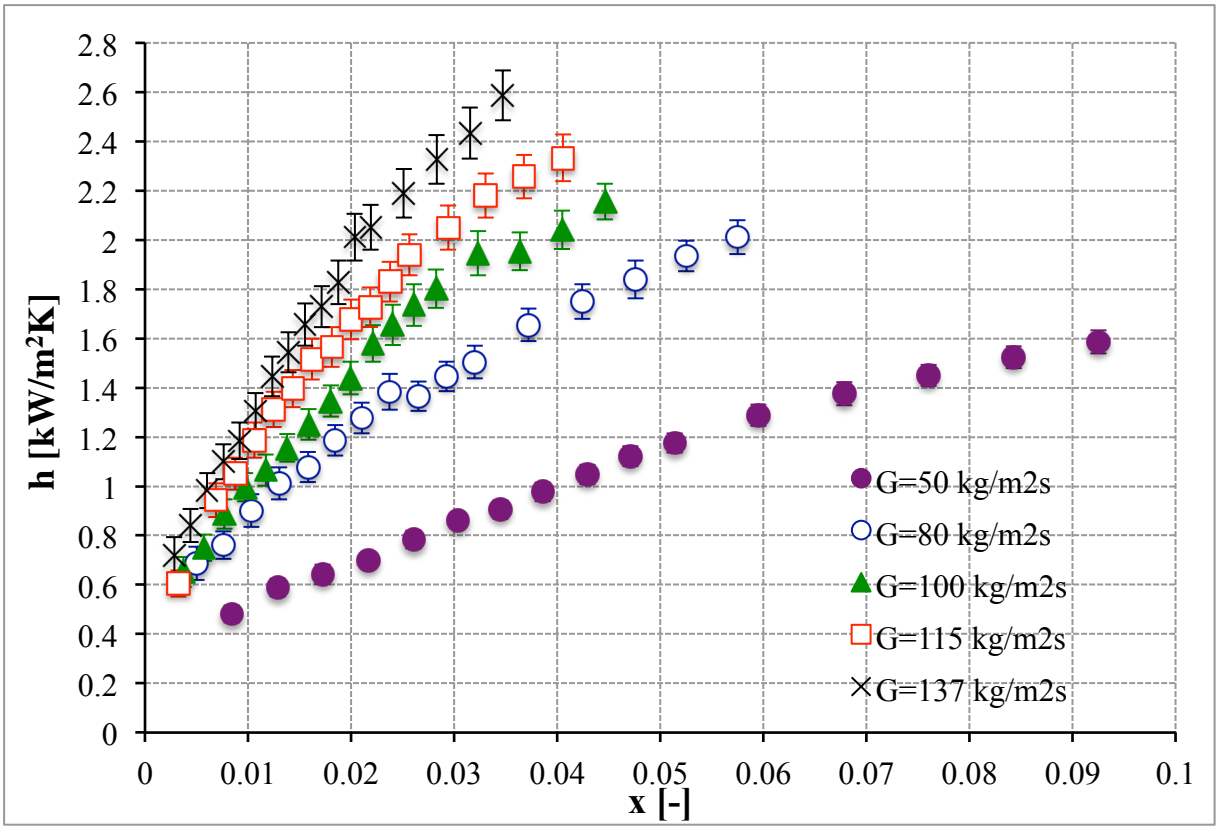

Figure 7 The heat transfer coefficient h, calculated from each boiling curve - obtained decreasing the heat flux - as function of the vapor quality.

The heat transfer coefficient, estimated at one fixed heat flux value or one wall superheat value, increases with the mass flux level. For such very low vapor qualities, the heat transfer coefficient increases with the vapor quality, meaning that more active bubbling (in terms of frequency and nucleation site density) is increasing the heat transfer from the wall. Note that this appears to be in contrast with many experimental studies, among which [19,20,21], which predict a decrease of the heat transfer coefficient with vapor quality.

A final important consideration is related to the comparison of the obtained heat transfer coefficient values with some common correlations of the literature, summarized in table 4, which are given in Figure 8 a,b,c.

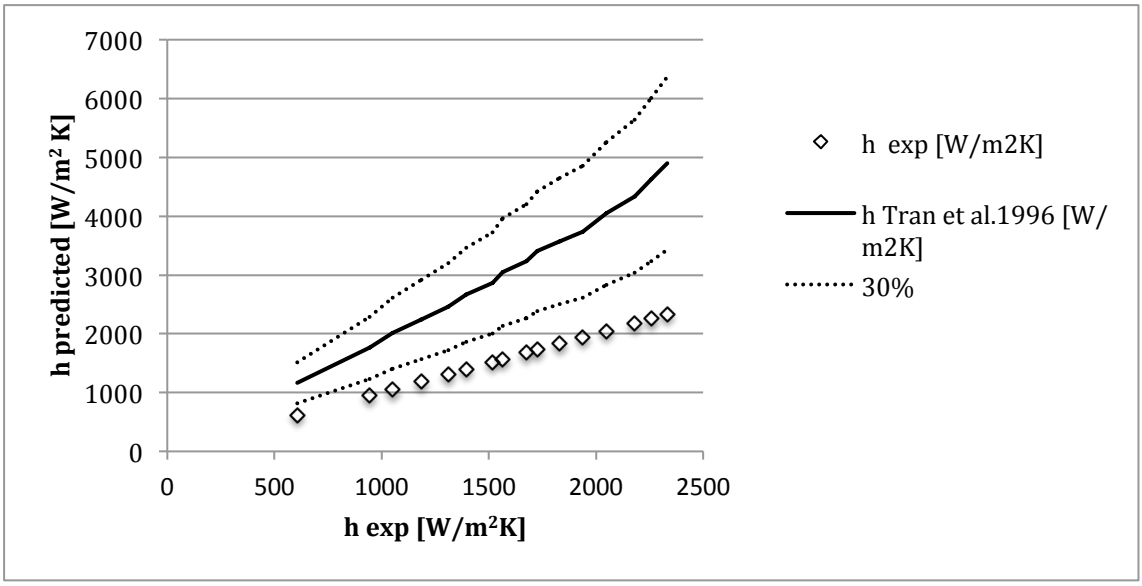
7000
6000
5000
4000
3000
2000
1000
0
0
500
1000
1500
2000
2500
h predicted [W/m² K]
h exp [W/m²K]
h exp [W/m2K]
h Tran et al.1996 [W/m2K]
30%

(a)

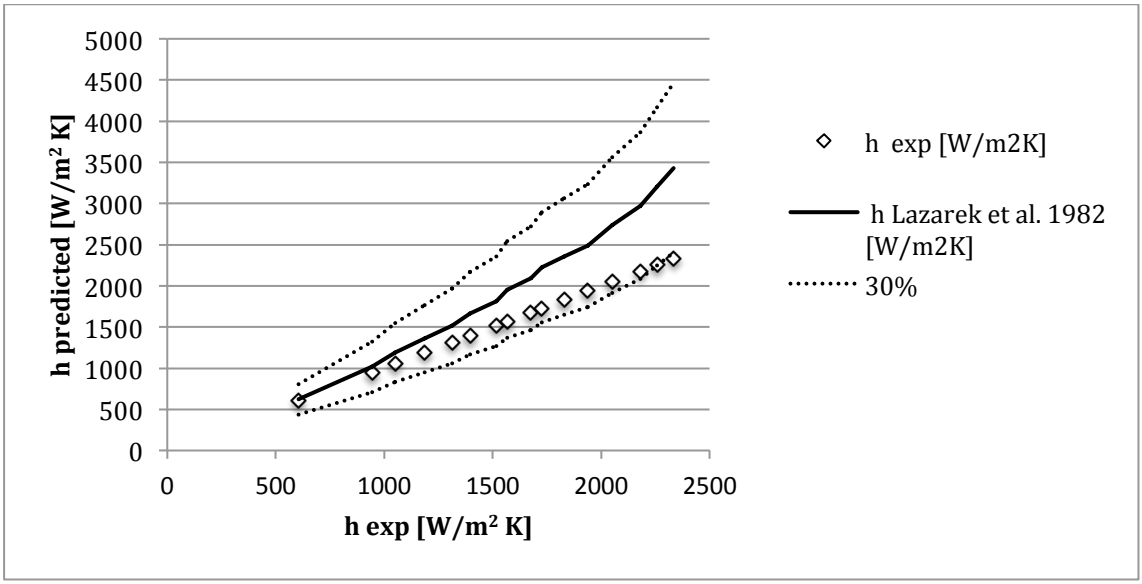
5000
4500
4000
3500
3000
2500
2000
1500
1000
500
0
0
500
1000
1500
2000
2500
h predicted [W/m² K]
h exp [W/m² K]
h exp [W/m2K]
h Lazarek et al. 1982 [W/m2K]
30%

(b)

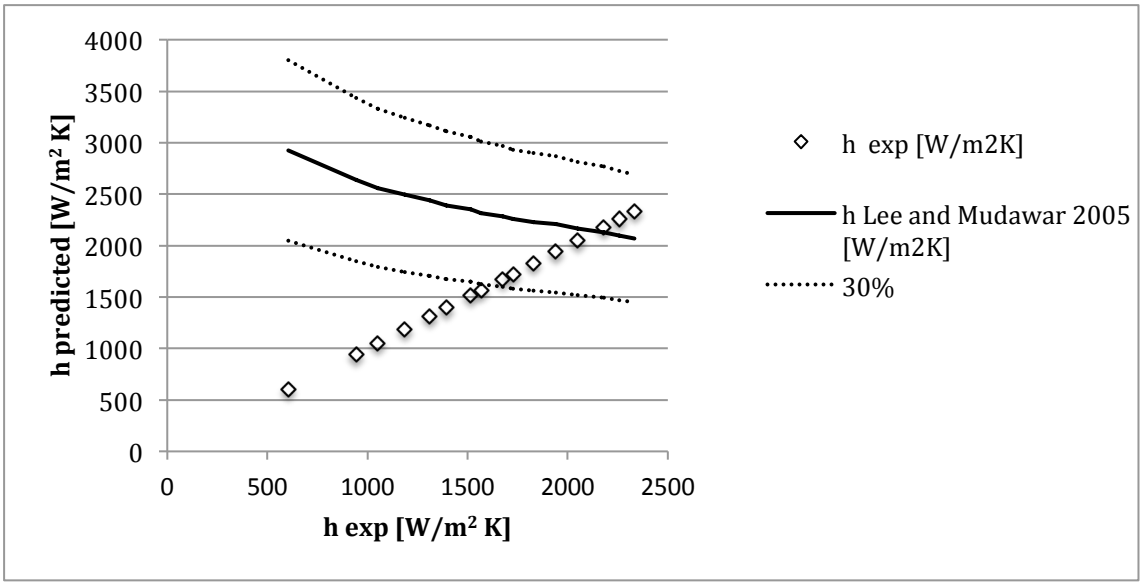

(c)

Figure 8 Comparison of the heat transfer coefficients, calculated from the experimental boiling curve decreasing the heat flux (G=115kg/m²s, vapor quality range 0<x<0.04, open symbols) with standard correlations in literature summarized in Table 4 (lines).

Name of the correlation	Equation and experimental range
Lazarek and Black [23]	$h = \left(30\,\mathrm{Re}_{LO}^{0.857}\,Bl^{0.714}\right)\frac{k_L}{d_h}$ R-113 $14<q''<380\,\mathrm{kW/m^2}$ $125<G<750\,\mathrm{kg/m^2s}$ $0<x<0.6$
Tran et al. [22]	$h = 8.4\cdot10^5\cdot\left(We_{LO}Bl^2\right)^{0.3}\left(\frac{\rho_L}{\rho_V}\right)^{-0.4}$ R-12 $3.6<q''<129\,\mathrm{kW/m^2}$ $44<G<832\,\mathrm{kg/m^2s}$ $0<x<0.94$
Lee and Mudawar [24]	$h = 3.856X^{0.267}h_L$ for x<0.05 R-134a, $159<q''<938\,\mathrm{kW/m^2}$ $127<G<654\,\mathrm{kg/m^2s}$

Table 4 The empirical correlations of Lazarek and Black [23], Tran et al [22] and Lee and Mudawar [24]

The correlations of Lazarek and Black [23] and Tran et al. [22] do not contain the vapor quality parameter. Therefore, since the present experiments have been done in a narrow range of vapor qualities, the correlation of Lee and Mudawar [24] was also considered. They proposed a correlation for the heat transfer coefficient for R-134a and water in three ranges of

vapor quality: $x<0.05$, $0.05<x<0.55$,$0.55<x<1$. The correlation for vapor quality lower than 0.05 was implemented in the comparison even if the heat flux range for such correlation is higher than 22 kW/m^2 (Figure 8). The heat transfer coefficient h_L for the liquid phase was calculated according to Shah correlation [25].

The measured heat transfer coefficient values are in good agreement with the correlation of Lazarek et al. [22], with larger deviations with respect to the correlation of Tran et al. [23], while a strong departure with the correlation of Lee and Mudawar [24] appears. This correlation, for vapor quality lower than 0.05, was in fact validated only for water and none of the R-134a data. For a heat flux up to 22 kW/m^2, the values of the heat transfer coefficients are strictly related to the increase of bubble number and frequency. The estimated values of the heat transfer coefficient appear to be lower than expected, interpolating data for higher vapor quality values. The use of a single thermocouple on the minichannel and the fact that the glass has a low thermal conductivity, partially motivate the under-evaluation of the heat transfer coefficient.

4. CONCLUSIONS

Saturated heterogeneous non-uniform flow boiling of R134a in horizontal mini-channel has been experimentally investigated at five different mass flux levels (50, 80, 100, 115 and 137 kg/m^{2}s) with particular attention on the visualization of the onset of nucleate boiling. The boiling curves evidence two different temperature drops and this is due to the fact that nucleation always starts in the upper side of the heaters and only increasing the heat flux, activating more nucleation sites, boiling starts later in the lower part of the heater. The flow pattern visualizations highlight this non-uniform boiling. The reason for such behavior is still under investigation and it should be also linked to the low thermal diffusivity of the glass, which is rarely used in flow boiling studies as tube material. The heat transfer coefficient has been estimated as function of the heat flux and of the wall superheat for all tested mass fluxes. It emerges that, as expected, the heat transfer coefficient values, estimated at a fixed heat flux value or wall superheat value, increases with the mass flux level. With such very low vapor quality values, the heat transfer coefficients appear to increase with the vapor quality, i.e. with the number and frequency of bubble detaching from the surface. The estimated values of the heat transfer coefficients are ranging from 500 W/m^{2}K to 2000 W/m^{2}K, slightly less than expected values, obtained from previous standard empirical correlations.

5. NOMENCLATURE

Bl Boiling number

d_h Hydraulic diameter, m

h Heat transfer coefficient, $W/m^2 K$

h_L Heat transfer coefficient for the liquid phase, $W/m^2 K$

k_L Liquid thermal conductivity, W/mK

q″ Heat flux, W/m^2

Q_{max} Maximum power supplied to the fluid, W

Re_{LO} Reynolds number for total flow assumed as liquid

T_{win} Internal temperature of the heated wall, K

T_{sat} Saturation temperature, K

We_{LO} Weber number for total flow assumed as liquid

x Vapour quality

X Martinelli parameter

ΔT_{sh} Wall superheat, K

ρ_L Liquid density, kg/m^3

ρ_V Vapor density, kg/m^3

ACKNOWLEDGEMENTS

The work was financed by Italian Ministry of Universities through the project PRIN 2009 "Experimental and Numerical Analysis of Two-Phase Phenomena in Microchannel Flows for Ground and Space Applications". We would like to acknowledge Dr. Stefano Dall'Olio for the experimental set-up in Dalmine, Dr. Stefano Zinna and Eng. Antonello Cattide for the help and the discussions.

REFERENCES

[1] J.R. Thome, Boiling in microchannels: a review of experiment and theory, *Int. J. Heat Fluid Flow*, 25, 128–139, 2004.

[2] J.R. Thome, State of the art overview of boiling and two-phase flows in microchannels. *Heat Transfer Engineering*, 27 (9), 4-19, 2006.

[3] G.P. Celata, *Single and two-phase flow heat transer in micropipes*. Proc. Symp. 5th European Thermal-Sciences Conference, The Nederlands. 2008.

[4] T. Harirchian and S.V. Garimella, Boiling Heat Transfer and Flow Regimes in Microchannels- A Comprehensive Understanding, *Journal of Electronic Packaging*, 133 (1), 011001-1/10, 2001.

[5] C. Baldassari and M. Marengo, Flow boiling in microchannels and microgravity, Progress in Energy and Combustion Science, 39**,** 1-36, 2013.

[6] D.B. Tuckerman and R.F.W. Pease, High-Performance Heat Sinking for VLSI, *IEEE Electron Device Lett.*, ELD-2(5), 126–129, 1981.

[7] S.M. Ghiaasiaan and R.C. Chedester, Boiling incipience in microchannels. *Int. J. Heat Mass Transfer*, 45, 4599–4606, 2002.

[8] C. Bang, S.H. Chang, W.P. Baek, Visualization of the subcooled flow boiling of R-134a in a vertical rectangular channel with an electrically heated wall. *Int. J. of Heat and Mass Transfer*, 47, 4349–4363, 2004.

[9] C.M. Callizo, B.P. Palm, W. Owhaib, Subcooled flow boiling of R-134a in vertical channels of small diameter. *International Journal of Multiphase Flow*, 33, 822– 832, 2007.

[10] D. Liu, P.S. Lee, S.V. Garimella, Prediction of the onset of nucleate boiling in microchannel flow. *International Journal of Heat and Mass Transfer*, 48, 5134–5149, 2005.

[11] G. Hong, X. Yan, Y.H. Yang, S. Liu, Y.P. Huang, Experimental study on onset of nucleate boiling in narrow rectangular channel under static and heaving conditions. Annals of Nuclear Energy , 39, 26–34, 2012.

[12] M. Piasecka, S. Hozejowska, M.E. Poniewski, Experimental evaluation of flow boiling incipience of subcooled fluid in a narrow channel, International Hournal of Heat and Fluid Flow, 25, 159-172, 2004.

[13] S. Dall'Olio, M. Marengo, Boiling of R134a inside a glass minichannel. A new statistical approach of flow pattern characterization based on flow visualization. *Int. J. Heat Mass Transfer*, 55, 1048-1065, 2012.

[14] E.W. Lemmon, M.L. Huber, M.O. McLinden, NIST Standard Reference Database 23: Reference Fluid Thermodynamic and Transport Properties-REFPROP, Version 8.0, National Institute of Standards and Technology, Standard Reference Data Program, Gaithersburg 2007.

[15] C.Baldassari, M. Mameli, M. Marengo, Experimental Analysis Of Heterogeneous Non Uniform Flow Boiling Of R-134a Inside A Glass Minichannel*,* Proc. Symp. ECI 8th International Conference on Boiling and Condensation Heat Transfer, 2012

374 [16] J.R.T. Seddon, H.J. Zandvliet, D. Lohse, Knudsen Gas Provides Nanobubble Stability,
375 *Phys. Rev. Lett*., 107 (11), 116101, 2011.
376 [17] J.R.T. Seddon, E.S. Kooij, B. Poelsema, H.J. Zandvliet, D. Lohse, Surface Bubble
377 Nucleation Stability, *Phys. Rev. Lett*. 106, 056101, 2011.
378 [18] C.U. Chan, C.D. Ohl, Surface Nanobubble Nucleation Visualized with TIRF
379 Microscopy, *arXiv*:1204.2633, 2012.
380 [19] Wambsganss, M. W., France, D. M., Jendrzejczyk, J. A., Tran, T. N., Boiling Heat
381 Transfer in a Horizontal Small-Diameter Tube, J. Heat Transfer, vol. 115, pp. 963–972,
382 1993.
383 [20] Lin, S., Kew, P. A., and Cornwell, K., Flow Boiling of Refrigerant R141B in Small
384 Tubes, Trans IChemE 79, part A, pp. 417–424, 2001.
385 [21] Yen,T.-H., Kasagi, N., and Suzuki,Y., Forced Convective Boiling Heat Transfer in
386 Microtubes at Low Mass and Heat Fluxes, Compact Heat Exchangers, A Festschrift on the
387 60th Birthday of Shah, R.K.. Eds. G. P. Celata, B. Thonon, A. Bontemps, and S. G.
388 Kandlikar, Edizioni ETS, Pisa, Italy, 2002.
389 [22] Tran T.N., Wambsganss M.W., France D.M. Small circular- and rectangular channel
390 boiling with two refrigerants. International Journal of Multiphase Flow; 22-3: pp.485–498,
391 1996.
392 [23] Lazarek G.M., Black S.H. Evaporative heat transfer, pressure drop and criticalheat
393 flux in a small vertical tube with R-113. International Journal of Heat and Mass Transfer,
394 25-7: pp.945-960, 1982.
395 [24] Lee, H.J. , Mudawar, I., Two-phase flow in high-heat-flux micro-channel heat sink for
396 refrigeration cooling applications: Part II—heat transfer characteristics, Int. J Heat Mass
397 Transfer, 48, pp.941-955, 2005.
398 [25] Shah M.M, A general correlation for heat transfer during film condensation inside of
399 pipes, Int. J. Heat and Mass Transfer, Vol. 22, pp. 547-556, 1979.